JACS
JOURNAL OF THE AMERICAN CHEMICAL SOCIETY
Article
pubs.acs.org/JACS

Intracellular Adenosine Triphosphate Deprivation through Lanthanide-Doped Nanoparticles

Jing Tian,[†,‡] Xiao Zeng,[‡] Xiaoji Xie,[‡] Sanyang Han,[‡] Oi-Wah Liew,[§] Yei-Tsung Chen,[§] Lianhui Wang,*[,†,∥] and Xiaogang Liu*[,‡,⊥]

[†]Laboratory of Advanced Materials, Fudan University, Shanghai 200433, China

[‡]Department of Chemistry, National University of Singapore, Singapore 117543, Singapore

[§]Cardiovascular Research Institute, Department of Medicine, National University of Singapore, National University Health System, Singapore 117599, Singapore

[∥]Key Laboratory for Organic Electronics & Information Displays, Institute of Advanced Materials, and Jiangsu National Synergistic Innovation Center for Advanced Materials (SICAM), Nanjing University of Posts & Telecommunications, Nanjing 210023, China

[⊥]Institute of Materials Research and Engineering, 3 Research Link, Singapore 117602, Singapore

Supporting Information

ABSTRACT: Growing interest in lanthanide-doped nanoparticles for biological and medical uses has brought particular attention to their safety concerns. However, the intrinsic toxicity of this new class of optical nanomaterials in biological systems has not been fully evaluated. In this work, we systematically evaluate the long-term cytotoxicity of lanthanide-doped nanoparticles ($NaGdF_4$ and $NaYF_4$) to HeLa cells by monitoring cell viability (mitochondrial activity), adenosine triphosphate (ATP) level, and cell membrane integrity (lactate dehydrogenase release), respectively. Importantly, we find that ligand-free lanthanide-doped nanoparticles induce intracellular ATP deprivation of HeLa cells, resulting in a significant decrease in cell viability after exposure for 7 days. We attribute the particle-induced cell death to two distinct cell death pathways, autophagy and apoptosis, which are primarily mediated via the interaction between the nanoparticle and the phosphate group of cellular ATP. The understanding gained from the investigation of cytotoxicity associated with lanthanide-doped nanoparticles provides keen insights into the safe use of these nanoparticles in biological systems.

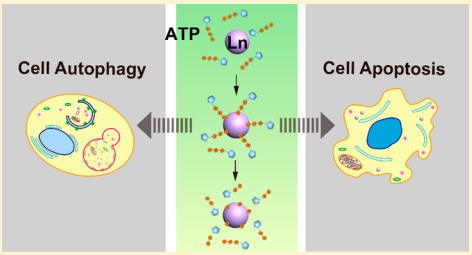

INTRODUCTION

Lanthanide-doped nanoparticles are an emerging class of nanomaterials that display intriguing luminescent and magnetic properties.[1] Among various types of lanthanide-doped nanoparticles, $NaGdF_4$- and $NaYF_4$-based nanoparticles have been widely applied in biomedical fields due to their multicolor emission feature and versatility for surface functionalization.[2] For example, $NaGdF_4$-based nanoparticles codoped with a sensitizer Yb^{3+} and different activators can emit tunable upconversion emissions via Gd-assisted energy migration and also serve as high contrast agents in magnetic resonance imaging (MRI) due to the T_1-weighted relaxivity of Gd.[3] Furthermore, when coupled with biomolecules or anticancer drugs, they would provide a multifunctional platform that combines labeling with diagnostics and therapy motifs in a highly integrated fashion.[4]

For biological applications, the biocompatibility of materials is always of paramount concern. Therefore, in vitro and in vivo toxicity assays of lanthanide-doped nanoparticles have routinely been carried out along with optical investigations of the materials. Until now, almost all previous investigations have shown that these nanoparticles have relatively low toxicity both in cells and in animal models.[5] However, many aspects of the intrinsic toxicity of the nanoparticles, for example, the exact mechanism of their toxicity, have yet to be established.

In previous studies, toxicity assays were usually conducted on nanoparticles coated with a thin layer of molecules such as poly(acrylic acid) (PAA), polyethylene glycol (PEG), silica, and proteins. The surface coating can greatly alter the dimensionality, morphology, and behavior of the nanoparticles, thereby interfering with accurate assessment of their toxicity profile. Considering that nanoparticles might undergo degradation within lysosomes and the coatings may be released in complex cellular environments, the intrinsic cytotoxicity of the naked nanoparticles should be emphasized regardless of the existence of surface passivation.[6] In addition, previous studies on nanoparticle cytotoxicity were typically conducted by incubating cells with nanoparticles over a time frame of 48 h. Evaluation of toxicity on the basis of such short-term assays is generally not well founded. Furthermore, previous methods for cytotoxicity assessment were often limited to single-mode assays, with MTT or MTS assay being the most commonly used. The results obtained from one single evaluation method may lead to data

Received: January 29, 2015

DOI: 10.1021/jacs.5b00981
J. Am. Chem. Soc. XXXX, XXX, XXX−XXX

misinterpretation.[7] In contrast, integrated multimode assays allow for cross-checking of experimental data obtained from various sources. Therefore, for precise and systematic evaluation of the intrinsic toxicity associated with lanthanide-doped nanoparticles, we propose that ligand-free nanoparticles be used as the benchmark model and that multiple approaches should be employed to track the health status of living organisms over a prolonged exposure period.

To this end, we conducted a series of cytotoxicity assessments on lanthanide-doped, ligand-free $NaYF_4$ and $NaGdF_4$ nanoparticles using a widely used human cervical cancer cell line (HeLa cells). Three different approaches, including MTS assay, ATP level determination, and lactate dehydrogenase (LDH) release measurement, were applied in parallel to evaluate the cytotoxicity of nanoparticles. With these three methods, we comprehensively measured cell conditions in terms of mitochondria activity, ATP concentration, and cell membrane integrity. These data would provide a more precise and balanced evaluation of nanoparticle-induced cytotoxcity than obtainable by a single MTS assay. Surprisingly, after cells were exposed to the nanoparticles for 3 days, we found that the intracellular ATP levels decreased dramatically while cell viability revealed by the MTS assay was not much affected. However, in a 7-day test, we observed severe reduction in cell viability, accompanied by even lower ATP levels than those obtained in the 3-day test. Our experimental results based on fluorescence microscopy, Western blotting, and Bio-TEM, etc., further indicated that the ligand-free nanoparticles can bind to the phosphate group of ATP and subsequently suppress cellular ATP levels, thereby inducing cell death via apoptosis and autophagy (Figure 1). By comparison,

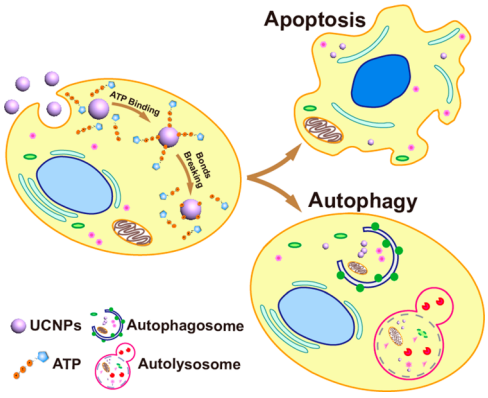

Figure 1. Schematic illustration of cell apoptosis and autophagy induced by lanthanide-doped nanoparticles via intracellular ATP deprivation. Lanthanide ions on the surface of nanoparticles can bind with phosphate groups of ATP molecules within cells. ATP molecules are subsequently hydrolyzed to cause an intracellular starving condition, which further leads to apoptosis and autophagy. Apoptosis is characterized by cell shrinkage, membrane blebbing, and nucleus condensation. In contrast, autophagy is a process in which unnecessary and dysfunctional cellular components are digested within autophagosomes and autolysosomes.

surface modification of the nanoparticles (e.g., PAA encapsulation) can effectively lower the toxicity by inhibiting close contact between the lanthanide ions and ATP molecules. These results should enable better mechanistic understanding of cytotoxicity induced by the lanthanide-doped nanoparticles and justify the necessity for surface coating with high levels of uniformity to minimize cytotoxic effects. Additionally, the intrinsic toxicity of these nanoparticles may offer new possibilities for improved anticancer therapy.[8]

EXPERIMENTAL SECTION

Chemicals and Reagents. Gadolinium(III) acetate hydrate (99.9%), yttrium(III) acetate hydrate (99.9%), ammonium fluoride (NH_4F, >98%), sodium hydroxide (NaOH, >98%), 1-octadecene (90%), oleic acid (90%), PAA, and adenosine 5′-triphosphate disodium salt hydrate were all supplied by Sigma-Aldrich.

Dulbecco's Modified Eagle Medium (DMEM), penicillin-streptomycin (10 000 U/mL), phosphate buffered saline (PBS), and fetal bovine serum (FBS) were obtained from Gibco. Rhodamine phalloidin and DAPI (4′,6-diamidino-2-phenylindole) were purchased from Molecular Probes. The dead cell apoptosis kit containing Annexin V-FITC and propidium iodide (PI) was from Invitrogen. Monodansylcadaverine (MDC) and anti-LC3B antibody were obtained from Sigma-Aldrich, and antiactin antibody was from Santa Cruz Biotechnology. Both secondary antibodies and all reagents for Western blotting were purchased from Bio-Rad. Kits for cytotoxicity measurements, including MTS assay, ATP level determination, LDH release, and caspase-3/7 detection, were all obtained from Promega Corp. Pierce bicinchoninic acid (BCA) protein assay was from Thermo Scientific (Rockford, IL).

All chemicals and agents were used without further purification unless otherwise noted.

Characterization. Transmission electron microscopy (TEM) measurements were conducted with a field emission transmission electron microscope (JEOL-JEM 2010F) coupled with an energy-dispersive X-ray spectrometer (EDX) with an Oxford INCA energy system. Fluorescence microscopy images were obtained with an inverted fluorescence microscope (Nikon Eclipse Ti). Inductively coupled plasma optical emission spectrometry (ICP-OES) measurement was performed on a Dual-view Optima 5300 DV ICP-OES system (PerkinElmer). UV−vis absorption spectra were obtained with a UV-3600 spectrophotometer (SHIMADZU). Fourier transform infrared (FTIR) spectroscopy was conducted on a Varian 3100 FT-IR spectrometer. The hydrodynamic size and zeta potential of nanoparticles in water and cell culture medium were measured on a Zetasizer Nano ZS90 (Malvern) instrument. X-ray diffraction (XRD) patterns of the nanoparticles were obtained on a Bruker D8 Advance diffractometer. Flow cytometry analysis was conducted on a BD LSRFortessa cell analyzer.

Preparation of Ligand-Free Nanoparticles. Oleic acid (OA) ligand molecules on the surface of nanoparticles were removed following a modified procedure described in the literature.[9] In a typical experiment, the as-synthesized oleic acid-capped lanthanide-doped nanoparticles (1 mL in cyclohexane) were precipitated out by adding 1 mL of ethanol and pelleted by centrifugation at 16 500 rpm for 5 min. After centrifugation, the supernatant was replaced with a solution comprised of 1 mL of hydrochloric acid (2 M) and 1 mL of ethanol, and the mixture was ultrasonicated for 5 min. The as-obtained nanoparticle-containing dispersion was then centrifuged at 16 500 rpm for 20 min to afford the ligand-free nanoparticles. The nanoparticles were further purified by washing with 2 mL of ethanol−water solution (1:1, v/v) several times and finally dispersed in Milli-Q water. The concentration of the nanoparticles in water was determined by drying 200 μL of the as-synthesized nanoparticles in an oven at 80 °C for 48 h and then weighing out the nanoparticles using an analytical balance.

Cytotoxicity Assays. HeLa cells were seeded at a density of 2000−5000 cells per well (100 μL) in 96-well plates and incubated for 24 h. Nanoparticle-containing cell culture medium (particle densities ranging from 0 to 1600 μg/mL) was subsequently added to the cells in the respective wells and further incubated for another 24−72 h. For the MTS assay, 20 μL of MTS reagent was added to each well of the microplate. After incubation for 4 h at 37 °C, the absorption of the colored formazan product at 490 nm was measured on a microplate reader. For ATP determination, 100 μL of CellTiter-Glo reagent equivalent to the volume of the cell culture medium in each well was added to the microplate followed by 2 min shaking on an orbital shaker to induce cell lysis. After a further 10 min incubation at room

DOI: 10.1021/jacs.5b00981
J. Am. Chem. Soc. XXXX, XXX, XXX−XXX

temperature to allow stabilization of the luminescent signals, determination of cellular ATP level as a function of the luminescence recorded was made. For the measurement of LDH release, 2 μL of lysis solution was added to three wells of cells cultured in the absence of nanoparticles to generate the maximum LDH release control, which allows estimation of the total number of cells in the well. One hundred microliters of assay reagents were added to nanoparticle-treated cells and incubated for 10 min at room temperature, followed by addition of stop solution (50 μL) to each well. Fluorescence signals of experimental, maximum LDH release, and culture medium background were recorded with excitation at 560 nm and emission at 590 nm. The amount of released LDH is determined as a percentage of the background-corrected fluorescence signals of the experimental groups versus the fluorescence signals of the maximum LDH release group.

For 7-day toxicity assays, HeLa cells were plated onto 24-well plates at a density of 5000 cells per well and then incubated with nanoparticles for 7 days. The nanoparticle-treated cells were dissociated from the well surface with 150 μL of trypsin/EDTA solution, followed by addition of 600 μL of culture medium to stop the reaction. Subsequently, 100 μL of cell suspension was transferred to 96-well plates for MTS assay, ATP level determination, and LDH release, respectively.

Annexin V/PI Staining. Apoptosis and necrosis of HeLa cells induced by lanthanide-doped nanoparticles were measured by an Annexin V-FITC/PI staining technique. Briefly, HeLa cells were first treated with different concentrations of ligand-free nanoparticles in 6-well plates for 3 and 7 days, respectively. The particle-treated cells were then trypsinized and centrifuged at 1000 rpm for 5 min, followed by washing with PBS. The washed cells were suspended with 100 μL of buffer provided from the staining kit and subsequently labeled with Annexin V-FITC/PI. The samples were analyzed with a flow cytometry analyzer with at least 10 000 cells counted for each analysis. The fluorescence signals obtained from flow cytometry serve to reflect the living status of cells. Specifically, under 488 nm laser excitation, early apoptotic cells only show green fluorescence (FITC+/PI-), while necrotic cells exclusively emit red fluorescence (FITC-/PI+). The absence of any fluorescence signal (FITC-/PI-) suggests that cells are viable, and the appearance of both green and red fluorescence (FITC +/PI+) indicates cells are in a late apoptotic stage.

MDC Staining. HeLa cells were exposed to different concentrations of ligand-free nanoparticles in 6-well plates for 3 and 7 days. The cells were then stained with 50 μM of MDC at 37 °C for 15 min and washed three times with PBS.

Western Blotting. After incubation with varied amounts (0, 100, 200, 400, 800, and 1600 μg/mL) of ligand-free nanoparticles, HeLa cells were trypsinized, isolated by centrifugation at 1000 rpm for 5 min, and lysed with RIPA buffer containing protease inhibitors. Subsequently, these lysed cells were centrifuged at 14 500 rpm for 20 min at 4 °C to afford clear lysate. The protein content of the cell lysate was determined using the BCA protein assay kit. All samples were diluted to 4 μg/μL with 2× Laemmli sample buffer and then boiled for 5 min. The samples were separated by polyacrylamide gel electrophoresis and transferred to a PVDF membrane. Next, the membrane was incubated in blocking buffer for 30 min and treated overnight with anti-LC3B antibody (1:1000× dilution) at 4 °C. After being washed with Tris-buffered saline (TBS: 0.05% Tween-20) five times, the membrane was further incubated with horseradish peroxidase-conjugated goat-antirabbit antibody (1:3000× dilution) for 1 h at room temperature. After being washed with TBS buffer, an enhanced chemiluminescence substrate in peroxide buffer (Clarity ECL Substrate, Bio-Rad) was used to visualize the immunoreactive proteins immobilized on the PVDF membrane.

Bio-TEM. HeLa cells were cultured in a T-25 flask containing 400 μg/mL of nanoparticles for 72 h before being collected for TEM sample preparation. Harvested cells were sequentially incubated with modified Karnovsky's fixative (2% paraformaldehyde and 2.5% gluteraldehyde in PBS) and OsO_4 (1%) for 1.5 h each to fix protein contents and lipids, respectively. Subsequently, the cells were dehydrated with ethanol solution and embedded in Spurr's resin. The samples were then cut into ultrathin sections, mounted on TEM grids, and stained with uranyl acetate and lead citrate for 10 min each prior to TEM characterization.

Statistical Analysis. For each experiment, at least three independent assays were performed. Data are expressed as mean ± standard deviation, and analyzed with analysis of variance followed by the Bonferroni post hoc test with $P < 0.05$ considered as significant difference.

RESULTS AND DISCUSSION

In this work, we implemented the cytotoxicity study using approximately 30 nm hexagonal $NaGdF_4$ and $NaYF_4$ nanoparticles (Supporting Information Figures S1 and S2). To reveal the intrinsic toxicity of lanthanide-doped nanoparticles, surface-coated oleic acid molecules were removed by acid treatment to afford the ligand-free nanoparticles (Supporting Information Figures S3 and S4). Dynamic light scattering (DLS) measurement suggests that positively charged ligand-free nanoparticles have a hydrodynamic diameter of around 45 nm. When dispersed in a cell culture medium, the positive charges of the nanoparticles were neutralized by negatively charged proteins and ions in the buffer. The hydrodynamic diameter was increased to about 250 nm, indicating the aggregation of the particles in the cell culture medium. By comparison, nanoparticles coated with PAA did not exhibit any noticeable signs of particle aggregation as evident by similar hydrodynamic diameter obtained in water and cell culture medium (Supporting Information Table S1).

To fully probe the cytotoxicity of the ligand-free nanoparticles under investigation, three types of analytical approaches in multiwell formats were used, MTS assay, ATP level measurement, and LDH leakage test (Figure 2, Supporting Information

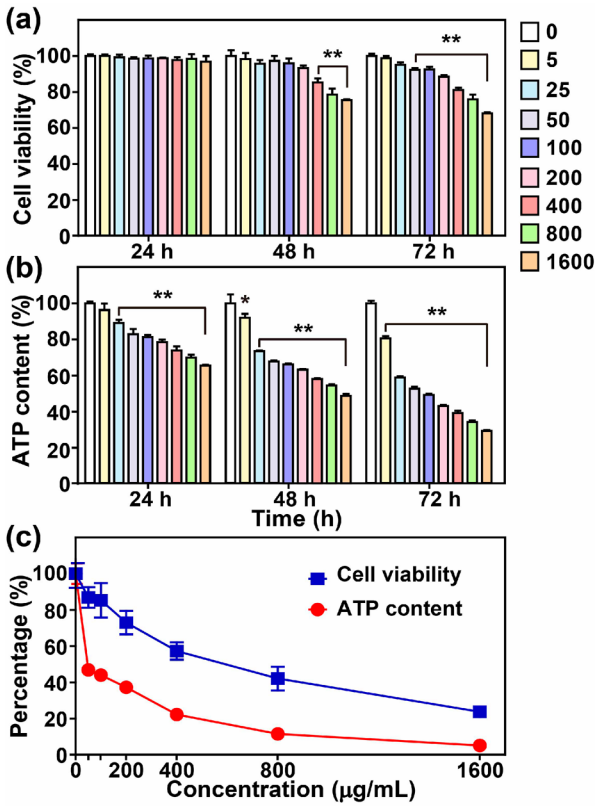

Figure 2. Cytotoxicity effect of ligand-free $NaGdF_4$ nanoparticles on HeLa cells. (a) MTS assay and (b) ATP level of the cells after 24, 48, and 72 h of exposure at dosages of 0−1600 μg/mL. (c) Cytotoxicity tests with MTS assay (blue line) and ATP level test (red line) after treatment with 0, 50, 100, 200, 400, 800, and 1600 μg/mL of the nanoparticles for 7 d. *$P < 0.05$, **$p < 0.01$.

DOI: 10.1021/jacs.5b00981
J. Am. Chem. Soc. XXXX, XXX, XXX−XXX

Figures S5 and S6). We first performed the most commonly used MTS assay whereby the reduction of MTS to generate colored formazan is assumed to reflect mitochondrial/NADH activity and hence cell viability. It was found that both $NaGdF_4$ and $NaYF_4$ nanoparticles essentially did not affect cell growth within 24 h even at all tested nanoparticle concentrations. A notable decrease in cell viability (≤80%) was found in groups treated with nanoparticles at concentrations above 400 μg/mL after 48-h incubation (Figure 2a and Supporting Information Figure S6a).

Although the cell viability as determined by the MTS assay was not significantly reduced, we surprisingly discovered that the cellular ATP content declined dramatically as a function of particle loading or incubation time after treatment with the ligand-free nanoparticles (Figure 2b and Supporting Information Figure S6b). For instance, cells treated with 400 μg/mL of nanoparticles retained about 70% and 40% of ATP level after incubation for 24 and 72 h, respectively. It should be noted that ATP molecules play a key role in the energy supply for cell metabolism and survival. Hence, our experimental observation on nanoparticle-induced ATP depletion explicitly indicates the negative impact of the ligand-free nanoparticles on cell growth and proliferation.

To further investigate the cytotoxicity of the ligand-free nanoparticles, cellular membrane integrity was measured with the LDH leakage assay, as the release of LDH molecules was triggered upon disruption of the cell membrane. It was found that intracellular LDH concentrations of the cells treated with ligand-free nanoparticles showed little difference with the untreated control group (Supporting Information Figures S5 and S6c). This indicates low adverse effects of the nanoparticles on cell membrane integrity within a time frame of 72 h.

Although cell viability remained high as revealed from mitochondrial activity in the 3-d experiment, the ATP content of the cells under investigation was no longer abundant. Consequently, HeLa cells were thought to be undergoing a metabolically starved condition, which is expected to affect the cell viability in the long term. To validate our hypothesis, we investigated the survival rate of the HeLa cells by culturing them with the ligand-free nanoparticles for an extended period of 7 days.

We observe that cell viability as reflected by MTS assay decreases significantly after incubation with ligand-free nanoparticles for 7 d (Figure 2c and Supporting Information Figure S6d). Specifically, by exposing cells to ligand-free nanoparticles with a concentration of 800 μg/mL, the cell viability was reduced from 75% at day 3 to 45% at day 7, and cellular ATP content dropped sharply to about 10%. These results suggested that a long-term treatment with ligand-free nanoparticles could induce a significant decrease of both cell viability and ATP level.

To further study the effect of ligand-free nanoparticles on HeLa cells, cell morphologies were screened under an optical microscope after particle treatment. Interestingly, cytoplasmic vacuolization (bubble-like structures) appeared in HeLa cells when exposed to the ligand-free nanoparticles at a high dose (1600 μg/mL) or over 2 days. In the 3- and 7-d treatment group, large vacuoles and membrane blebbing could be observed in the cells treated with over 400 μg/mL of the nanoparticles (Figure 3, Supporting Information Figures S7 and S8).

We also performed fluorescence microscopy to image the cells by staining cytoskeletal structures (actin) and nuclei with rhodamine phalloidin and DAPI, respectively. It could be seen that after particle treatment for more than 3 days, a number of cells exhibited shrunken or inflated morphologies, accompanied

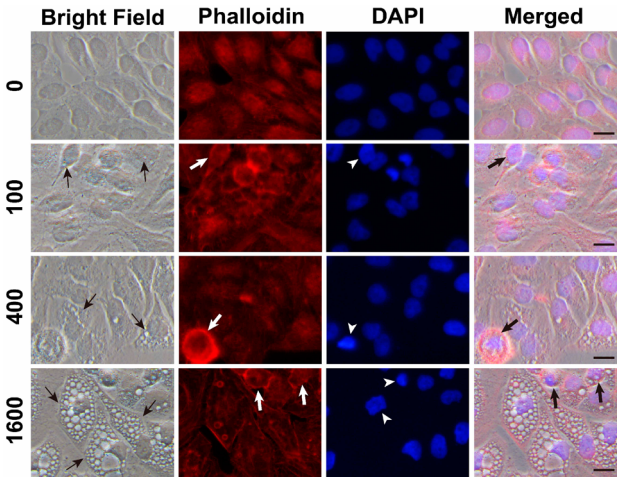

Figure 3. Effects of ligand-free $NaGdF_4$ nanoparticles on HeLa cell morphology. Cells were treated with the nanoparticles at 0, 100, 400, and 1600 μg/mL for 7 d and then stained with rhodamine palloidin and DAPI for actin and nuclei, respectively. Morphological alterations include cytoplasmic vacuolization (black arrows), cell shrinkage (white and thick black arrows), and nucleus condensation and irregularity (arrowheads). All photos were taken under identical settings. Scale bars are 20 μm.

by the formation of condensed, irregular, or fragmented nuclei within the cells (Figure 3 and Supporting Information Figures S9−11). Cytoplasmic vacuolization was considered to correlate with cell autophagy, while membrane blebbing and nuclear condensation were associated with apoptosis.[10] Therefore, these results provided indications that cells might be undergoing programmed cell death after ligand-free nanoparticle treatment.

Generally, there are three typical pathways of cell death, necrosis, apoptosis, and autophagy.[10] When ATP is in short supply, autophagy would be activated to isolate damaged organelles and cytoplasmic materials in autolysosomes. Autophagic degradation produces fatty and amino acids that can be used for ATP synthesis to sustain cell survival under ATP-deficient conditions.[11] The dramatic decrease in ATP content in our tests prompted us to examine whether autophagy was triggered in these nanoparticle-treated cells.

To investigate the possibility of autophagy, we stained HeLa cells with a typical autophagy-reporting dye monodansylcadaverine (MDC).[12] The fluorescence microscopy image showed that the green signals of MDC intensified with increasing doses of nanoparticles after 3- and 7-d treatment, suggesting the occurrence of autophagy in the presence of nanoparticles (Figure 4a,b and Supporting Information Figure S12). In addition to MDC staining, during autophagy, microtubule-associated protein (Light Chain 3: LC3) can be lipidated from LC3-I (18 kDa) to LC3-II (16 kDa), making it ideal as markers for the cell death study.[12] Therefore, we measured the conversion of LC3 by Western blotting and found that the intensity of the LC3-II immunodetected protein band steadily increased with increase in the particle concentration from 100 to 1600 μg/mL (Figure 4c,d and Supporting Information Figure S12). Obviously, the ratios of LC3-II/LC3-I are much higher in the cells exposed for 7 d, indicating the time-dependent autophagy process of the cells.

To further validate the existence of autophagy, TEM images were taken to examine cells after particle treatment. Two types of autophagic vacuoles, autophagosomes (initial autophagic vacuoles with intact organelles or cytoplasmic materials) and autolysosomes (late/degradative autophagic vacuoles containing

DOI: 10.1021/jacs.5b00981
J. Am. Chem. Soc. XXXX, XXX, XXX−XXX

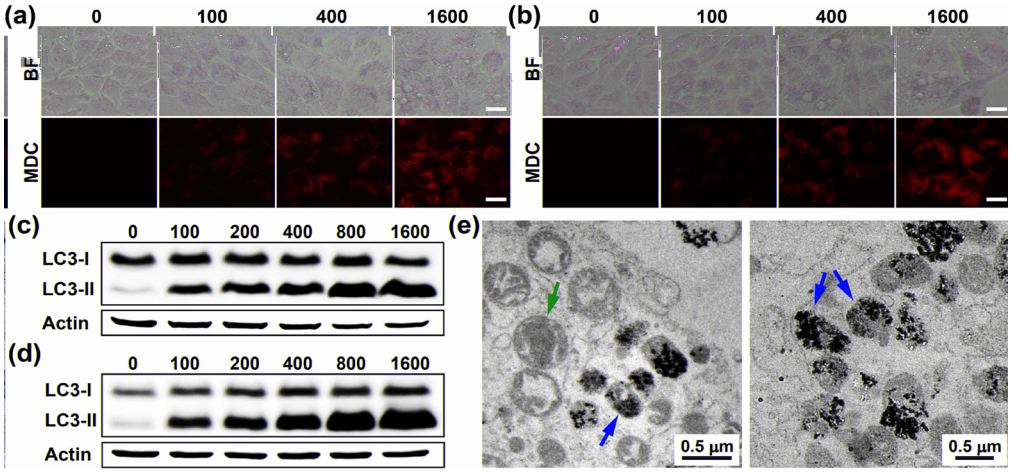

Figure 4. Cell autophagy induced by ligand-free $NaGdF_4$ nanoparticles. (a,b) Fluorescence microscopy of HeLa cells with MDC staining after exposure to 0, 100, 400, and 1600 μg/mL of nanoparticles for 3 d (a) and 7 d (b), respectively. All photos were taken under identical settings (scale bar: 20 μm). (c,d) Expression of LC3 protein by Western blotting. HeLa cells were treated with 0, 100, 200, 400, 800, and 1600 μg/mL of nanoparticles for 3 d (c) and 7 d (d), respectively. Actin is used as loading control. (e) TEM imaging analysis of the HeLa cells after exposure to the $NaGdF_4$ nanoparticles. Blue and red arrows marked in the TEM images indicate autophagosomes and autolysosomes, respectively.

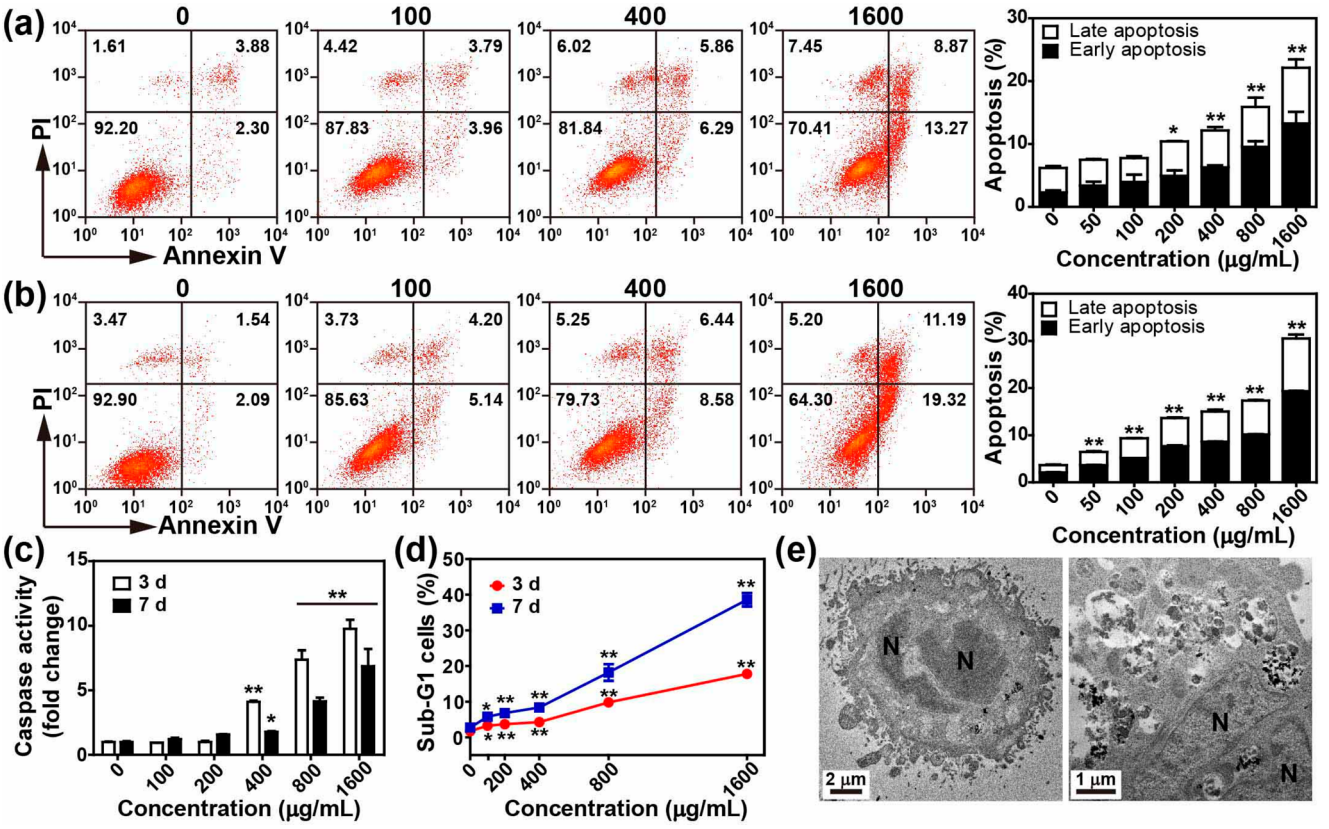

Figure 5. Effects of ligand-free $NaGdF_4$ nanoparticles on HeLa cell apoptosis. (a,b) Representative profiles of fluorescence activated cell sorting analysis and statistical results of early and late apoptosis at day 3 (a) and day 7 (b) after exposure to 0, 50, 100, 200, 400, 800, and 1600 μg/mL of $NaGdF_4$ nanoparticles. (c) Fold changes of caspase-3/7 expression after treatment with nanoparticles for 3 and 7 d as compared to untreated groups. (d) DNA fragmentation by measuring cells in sub-G1 phase with flow cytometry after nanoparticle treatment for 3 and 7 d. (e) Bio-TEM images of apoptotic cells with fragmented and irregular nuclei (N). *$P < 0.05$, **$p < 0.01$.

partially degraded organelles and cytosolic materials),[12,13] were both observed within these cells, confirming the nanoparticle-induced autophagic cell death pathway (Figure 4e). In addition, nanoparticles with cell debris were observed within the autolysosomes, suggesting that nanoparticles might be digested during the process of autophagy. Taken together, MDC staining results, Western blotting analysis, and bio-TEM images provide evidence of the autophagy pathway occurring in the cells incubated with ligand-free nanoparticles.

It should be noted that different cell death pathways can coexist upon external stimulation. For example, CeO_2 nanoparticles have been demonstrated to trigger both autophagy and

DOI: 10.1021/jacs.5b00981
J. Am. Chem. Soc. XXXX, XXX, XXX−XXX

apoptosis simultaneously.[14] To provide insights into the cell death mechanism induced by ligand-free nanoparticles, we conducted flow cytometry analysis to ascertain whether apoptosis or necrosis takes place in our nanoparticle-modified cells.

In necrosis, the cell membrane is ruptured, allowing for the uptake of nonpermeable dyes such as propidium iodide (PI) for cell staining. In contrast, apoptotic cells maintain membrane integrity in the early stage, prohibiting nonpermeable dye PI from entering cells. Meanwhile, apoptotic cells can be distinguished by staining cells using annexin V, a cellular protein that can bind to phosphatidylserine externalized particularly in the apoptotic cell membrane.[15] With PI and annexin V double staining, we can distinguish healthy cells (annexin V−/PI−), early apoptotic cells (annexin V+/PI−), late apoptotic cells (annexin V+/PI+), and necrotic cells (annexin V−/PI+). As shown in Figure 5, the percentage of early apoptotic cells was approximately 13% after treatment with 1600 μg/mL ligand-free nanoparticles at day 3, and the percentage further increased to 19% at the end of day 7. In contrast, for the control group with zero exposure to nanoparticles, only 2% of the cells underwent apoptosis. Statistically, treatment with more than 200 μg/mL of nanoparticles induced significant apoptosis as compared to the control group after 3 d, and all particle-treated groups experienced significant apoptosis at day 7 (Figure 5a,b and Supporting Information Figure S13). In contrast, no obvious necrosis was detectable, and this observation was consistent with the results of the LDH assays.

During apoptosis, one class of cysteine proteases named caspases will be activated to initiate and regulate apoptotic signaling. Although there are different regulatory pathways of apoptosis regulation, they will converge at the same terminal point with caspase-3 and caspase-7 being activated.[16] As shown in Figure 5c and Supporting Information Figure S13, caspase-3 or caspase-7 were highly expressed in nanoparticle-treated cells ($\geq$400 μg/mL) as compared to the control group. It should be noted that no significant levels of caspase-3 or caspase-7 could be detected at low concentrations of nanoparticles. This is probably because caspases were only expressed transiently within the cells for a short period of time and low concentrations of ligand-free nanoparticles are not sufficient to trigger the expression of caspases to detectable levels.[16]

In addition to probing apoptosis with protein markers, cellular apoptosis can also be studied by examining DNA content within the cells. During apoptosis, DNA strands are degraded by endonucleases into small fragments. Consequently, an increasing population of hypodiploid cells, which possess incomplete cellular DNA content, would be observed in cell cycle assays.[17] Not surprisingly, our data from cell cycle experiments clearly showed that treatment with nanoparticles increased the percentage of the hypodiploid cells, probably as a result of apoptosis (Figure 5d and Supporting Information Figure S13). Furthermore, irregular and fragmented nuclei in the particle-treated cells were also observed from TEM imaging (Figure 5e). Collectively, the results from flow cytometry analysis, caspase expression, cell cycle assays, and TEM characterization all indicated that the ligand-free nanoparticles induced apoptosis in a time- and dose-dependent fashion.

To reveal the underlying mechanism leading to ATP deprivation by ligand-free lanthanide-doped nanoparticles, we studied the interaction between ATP and the nanoparticles in cell culture medium. After the nanoparticles were mixed with ATP-containing cell culture medium, the ATP molecules were detected by the same method as that used in the in vitro experiments. The viable ATP concentration decreased remarkably in a dose- and time-dependent manner (Figure 6a and Supporting Information Figure S14a). Specifically, 100 μg/mL of ligand-free nanoparticles caused over 40% reduction in ATP content after 24 h incubation, and the ATP concentration continued declining with increasing incubation time. Furthermore, we examined the variation in the concentration of adenosine, which forms the basis of ATP molecules, in response to particle incubation. In this experiment, the nanoparticle−ATP mixture was first centrifuged at 16 500 rpm for 20 min, and the concentration of adenosine in the supernatant was subsequently measured by a UV−vis spectrometer. Interestingly, the adenosine concentration remained unchanged in the presence of ligand-free nanoparticles despite the decrease in viable ATP (Figure 6b and Supporting Information Figure S14b). HPLC analysis was conducted to examine the composition of the reaction product upon incubation of ligand-free nanoparticles with ATP for 24 h. It was found that in the presence of nanoparticles (400 μg/mL), approximately 60% of ATP molecules were decomposed into ADP and AMP, while the control group showed little sign of ATP hydrolysis (Supporting Information Figure S15). This degree of particle-mediated ATP decomposition is even aggravated when free lanthanide ions gradually leach from the nanocrystals (Supporting Information Figure S16). Therefore, we concluded that upon coordination to the phosphate groups of ATP by the nanoparticles and the free lanthanide ions, the cleavage of phosphate groups leads to the release of adenosine into the surroundings, while the phosphate groups remain on the surface of nanoparticles, as illustrated in Figure 6c and Supporting Information Figure S14c. Consequently, the ATP level decreased gradually, and the energy required for metabolic processes was subsequently drained.

To further illustrate the interaction between the ligand-free nanoparticles and ATP, we examined the nanoparticles

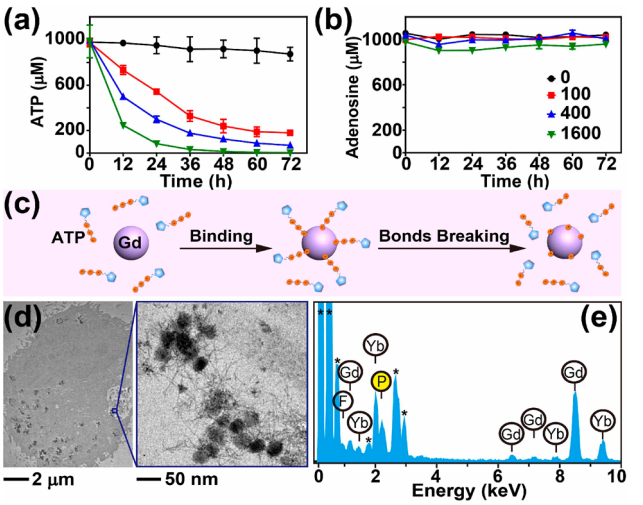

Figure 6. Investigation of the interaction of $NaGdF_4$ nanoparticles with ATP. (a) ATP and (b) adenosine concentration measurements after treatment with ligand-free $NaGdF_4$ nanoparticles at concentrations of 0, 100, 400, and 1600 μg/mL for 72 h. (c) Schematic illustration of the interaction between $NaGdF_4$ nanoparticles and ATP. (d) TEM characterization of cellular uptake of $NaGdF_4$ nanoparticles in HeLa cells. (e) EDX spectra of internalized $NaGdF_4$ nanoparticles (asterisks denote the elemental content of the cells, and phosphorus is highlighted in yellow).

DOI: 10.1021/jacs.5b00981
J. Am. Chem. Soc. XXXX, XXX, XXX−XXX

internalized by HeLa cells via TEM imaging analysis. As shown in Figure 6d, we observed the formation of needle-like bundles, which could be attributed to phosphate complexation by the nanoparticles after cellular uptake.[18] The existence of elemental phosphorus in these particles was confirmed by EDX analysis (Figure 6e).

In view of the above results, we believe that the ligand-free nanoparticles can trigger the decomposition of ATP molecules and thus lead to energy shortages within the cells under investigation. Without sufficient energy supply, autophagy and apoptosis can occur ubiquitously. To verify our hypothesis, we conducted an ATP rescue test by supplying additional ATP molecules to the cells treated with ligand-free nanoparticles (Supporting Information Figure S17). After being exposed to nanoparticles for 3 d, the cells were supplemented with extra ATP molecules in the cell medium and further incubated for 24 h. In the presence of additional ATP molecules, cell viability was increased by 3.3% (100 μg/mL group) and 16.1% (1600 μg/mL group) as compared to that obtained without the ATP supplement. On the contrary, in the absence of the nanoparticles, no obvious changes in cell proliferation were observed after addition of ATP molecules. Taken together, these results proved that addition of exogenous ATP molecules could partly offset the ATP deprivation caused by nanoparticles and rescue cells from cell death to a limited extent.

It is important to note that many other phosphate-containing biomolecules could interact with rare earth ions. For instance, rare earth oxides could damage lysosomes by stripping phosphates from lysosomal phospholipids and ensuingly activate inflammatory pathways.[18c] On a separate note, DNA can also bind to lanthanide-doped nanoparticles under cell-free conditions. However, the nanoparticles under investigation are not likely to enter nucleus and mitochondria because of the relatively large size of the nanoparticles. Despite unclear mechanisms underlying the interaction between the lanthanide-doped nanoparticles with other phosphate containing chemicals, the lack of vital energy currency in the form of ATP is expected to play an important role in the observed cell death.

From the foregoing, we show that the bare nanoparticles could interact with phosphate groups of ATP, leading to a decline in cellular ATP levels, and subsequently trigger autophagy and apoptosis. To suppress this interaction, we coated PAA on the surface of nanoparticles to block the direct interaction between ATP and ligand-free nanoparticles. We first conducted extracellular studies of the interaction between PAA-coated nanoparticles and ATP. It was obvious that the PAA-coated nanoparticles ($NaGdF_4$/PAA and $NaYF_4$/PAA) showed decreased binding affinity to ATP (Figure 7a and Supporting Information Figure S18).

Thereafter, we treated cells with $NaGdF_4$/PAA and $NaYF_4$/PAA for cytotoxicity tests. As expected, both $NaGdF_4$/PAA and $NaYF_4$/PAA displayed fairly low cytotoxicity based on MTS assay. An obvious reduction of cell viability was noticed only when nanoparticles were introduced at the highest concentration (1600 μg/mL) (Supporting Information Figure S19). In addition, the PAA coating helps maintain the cellular ATP content as reflected by ATP measurement. As shown in Figure 7b, cells incubated with $NaGdF_4$/PAA exhibited a gentler decline in their ATP levels as compared to cells exposed to ligand-free $NaGdF_4$ nanoparticles.

The protective effect of PAA coatings was also demonstrated in long-term viability assays (Figure 7c,d and Supporting Information Figure S20). Approximately 70% of cells were

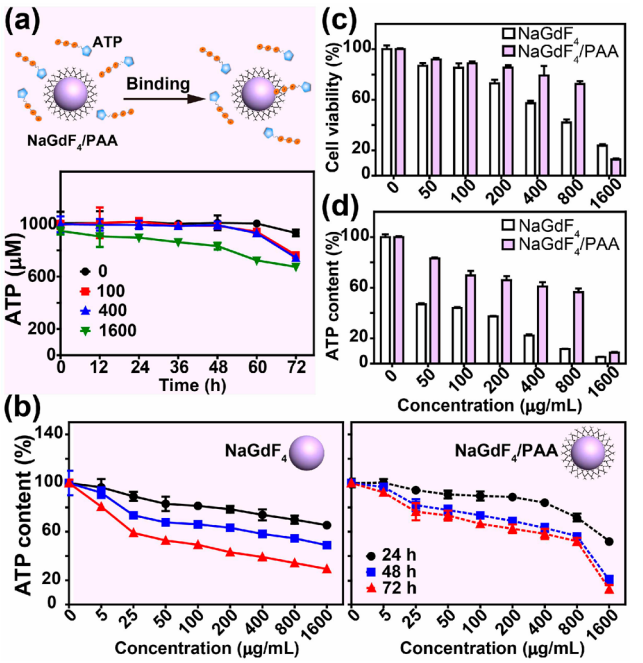

Figure 7. Protecting effects of PAA coatings on nanoparticle-induced cytotoxicity. (a) ATP concentration determination after binding with $NaGdF_4$/PAA nanoparticles at concentrations of 0, 100, 400, and 1600 μg/mL for 72 h. (b) Comparison of cellular ATP levels after 3-d exposure to $NaGdF_4$ or $NaGdF_4$/PAA nanoparticles at 0−1600 μg/mL. (c) MTS assays and (d) ATP tests of HeLa cells after treatment with $NaGdF_4$ or $NaGdF_4$/PAA nanoparticles at doses of 0, 50, 100, 200, 400, 800, and 1600 μg/mL for 7 d.

alive after incubating with 800 μg/mL PAA-coated nanoparticles for 7 d, as compared to a survival rate of 50% in the ligand-free group. Cells also maintained high ATP levels after a 7-d treatment with PAA-coated nanoparticles, suggesting that PAA-coatings can prevent ATP depletion over the longer term. Furthermore, the morphology of cells treated with $NaGdF_4$/PAA did not show obvious changes with dosages up to 400 μg/mL (Supporting Information Figure S21). When compared to ligand-free equivalents, PAA-coated nanoparticles exhibited lower cytotoxicity, despite the slightly higher level of cellular uptake of PAA-coated nanoparticles than their ligand-free counterparts (Supporting Information Figure S22). This result further confirms the shielding effect of the PAA coating. However, it is noted that the highest dose (1600 μg/mL) of the $NaGdF_4$/PAA induced a remarkable decrease of cell viability and ATP content, and resulted in cell shrinkage and cell death after 72-h treatment. This is probably caused by partial detachment of PAA molecules coated on the surface of nanoparticles over a prolonged period of time (Supporting Information Figure S23). When the concentration of nanoparticles is too high, partial dissociation of PAA from nanoparticle can leave enough lanthanide ions to bind with ATP and consequently cause cell death.

CONCLUSIONS

Controlling the surface properties of lanthanide-doped upconversion nanocrystals has major implications for applications in biological fields. In previous studies, the upconversion nanoparticles were typically coated with silica, PAA, PEG, or protein as model systems for toxicity investigations. As such surface modifications prevent the nanoparticles from binding to ATP,

DOI: 10.1021/jacs.5b00981
J. Am. Chem. Soc. XXXX, XXX, XXX−XXX

their intrinsic cytotoxicity cannot be fully disclosed. Herein, we have demonstrated that without the surface protection, lanthanide-doped nanoparticles do exhibit considerable cytotoxicity, largely due to ATP deprivation induced by strong binding between the lanthanide ions and the phosphate group of intracellular ATP. On the basis of our experimental findings, surface coatings (e.g., PAA) can effectively decrease the toxicity effect by preventing the interaction of nanoparticles with ATP. For long-term use of lanthanide-doped nanoparticles, the best practice is to limit their concentration to less than 100 μg/mL sufficient for cell imaging (Supporting Information Figure S24). These findings should provide improved fundamental understanding of the intrinsic toxicity associated with lanthanide-based nanomaterials in biological settings. Moreover, our results provide new insights for exploring the safe uses of these optical nanomaterials in advanced biological applications.

■ ASSOCIATED CONTENT

Supporting Information

Additional experimental details. The Supporting Information is available free of charge on the ACS Publications website at DOI: 10.1021/jacs.5b00981.

■ AUTHOR INFORMATION

Corresponding Authors

*iamlhwang@njupt.edu.cn

*chmlx@nus.edu.sg

Notes

The authors declare no competing financial interest.

■ ACKNOWLEDGMENTS

This study was supported by the Agency for Science, Technology, and Research through JCO Project (no. 1231AFG028) and Program for Changjiang Scholars and Innovative Research Team at the University of China (IRT1148). We thank R.D. and X.L. for helpful discussions. J.T. is grateful to the Chinese Scholarship Council for financial support.

■ REFERENCES

(1) (a) Gorris, H. H.; Wolfbeis, O. S. *Angew. Chem., Int. Ed.* **2013**, *52*, 3584. (b) Haase, M.; Schäfer, H. *Angew. Chem., Int. Ed.* **2011**, *50*, 5808. (c) Zhou, J.; Liu, Z.; Li, F. *Chem. Soc. Rev.* **2012**, *41*, 1323. (d) Wang, F.; Liu, X. *Chem. Soc. Rev.* **2009**, *38*, 976. (e) Teng, X.; Zhu, Y.; Wei, W.; Wang, S.; Huang, J.; Naccache, R.; Hu, W.; Tok, A. I. Y.; Han, Y.; Zhang, Q.; Fan, Q.; Huang, W.; Capobianco, J. A.; Huang, L. *J. Am. Chem. Soc.* **2012**, *134*, 8340. (f) Naccache, R.; Vetrone, F.; Mahalingam, V.; Cuccia, L. A.; Capobianco, J. A. *Chem. Mater.* **2009**, *21*, 717. (g) Wang, F.; Han, Y.; Lim, C. S.; Lu, Y.; Wang, J.; Xu, J.; Chen, H.; Zhang, C.; Hong, M.; Liu, X. *Nature* **2010**, *463*, 1061. (h) Johnson, N. J. J.; Korinek, A.; Dong, C.; van Veggel, F. C. J. M. *J. Am. Chem. Soc.* **2012**, *134*, 11068. (i) Xie, X.; Gao, N.; Deng, R.; Sun, Q.; Xu, Q.-H.; Liu, X. *J. Am. Chem. Soc.* **2013**, *135*, 12608. (j) Gai, S.; Li, C.; Yang, P.; Lin, J. *Chem. Rev.* **2014**, *114*, 2343. (k) Zhang, Y.; Zhang, L.; Deng, R.; Tian, J.; Zong, Y.; Jin, D.; Liu, X. *J. Am. Chem. Soc.* **2014**, *136*, 4893. (l) Mai, H.-X.; Zhang, Y.-W.; Si, R.; Yan, Z.-G.; Sun, L.-d.; You, L.-P.; Yan, C.-H. *J. Am. Chem. Soc.* **2006**, *128*, 6426. (m) Lai, J.; Zhang, Y.; Pasquale, N.; Lee, K. B. *Angew. Chem., Int. Ed.* **2014**, *53*, 14419. (n) Deng, R.; Qin, F.; Chen, R.; Huang, W.; Hong, M.; Liu, X. *Nat. Nanotechnol.* **2015**, *10*, 237. (o) Liu, X.; Yan, C.-H.; Capobianco, J. A. *Chem. Soc. Rev.* **2015**, *44*, 1299.

(2) (a) Wang, L.; Yan, R.; Huo, Z.; Wang, L.; Zeng, J.; Bao, J.; Wang, X.; Peng, Q.; Li, Y. *Angew. Chem., Int. Ed.* **2005**, *44*, 6054. (b) Zhang, F.; Shi, Q.; Zhang, Y.; Shi, Y.; Ding, K.; Zhao, D.; Stucky, G. D. *Adv. Mater.* **2011**, *23*, 3775. (c) Li, L.-L.; Zhang, R.; Yin, L.; Zheng, K.; Qin, W.; Selvin, P. R.; Lu, Y. *Angew. Chem., Int. Ed.* **2012**, *51*, 6121. (d) Deng, R.; Xie, X.; Vendrell, M.; Chang, Y.-T.; Liu, X. *J. Am. Chem. Soc.* **2011**, *133*, 20168. (e) Wang, J.; Deng, R.; MacDonald, M. A.; Chen, B.; Yuan, J.; Wang, F.; Chi, D.; Andy Hor, T. S.; Zhang, P.; Liu, G.; Han, Y.; Liu, X. *Nat. Mater.* **2014**, *13*, 157. (f) Liu, Y.; Chen, M.; Cao, T.; Sun, Y.; Li, C.; Liu, Q.; Yang, T.; Yao, L.; Feng, W.; Li, F. *J. Am. Chem. Soc.* **2013**, *135*, 9869. (g) Tu, D.; Liu, L.; Ju, Q.; Liu, Y.; Zhu, H.; Li, R.; Chen, X. *Angew. Chem., Int. Ed.* **2011**, *50*, 6306. (h) Nyk, M.; Kumar, R.; Ohulchanskyy, T. Y.; Bergey, E. J.; Prasad, P. N. *Nano Lett.* **2008**, *8*, 3834. (i) Wang, J.; Wang, F.; Wang, C.; Liu, Z.; Liu, X. *Angew. Chem., Int. Ed.* **2011**, *50*, 10369. (j) Liu, Y.; Ai, K.; Liu, J.; Yuan, Q.; He, Y.; Lu, L. *Angew. Chem., Int. Ed.* **2012**, *51*, 1437. (k) Yang, Y.; Shao, Q.; Deng, R.; Wang, C.; Teng, X.; Cheng, K.; Cheng, Z.; Huang, L.; Liu, Z.; Liu, X.; Xing, B. *Angew. Chem., Int. Ed.* **2012**, *51*, 3125. (l) Zhang, F.; Braun, G. B.; Pallaoro, A.; Zhang, Y.; Shi, Y.; Cui, D.; Moskovits, M.; Zhao, D.; Stucky, G. D. *Nano Lett.* **2012**, *12*, 61. (m) Jayakumar, M. K. G.; Idris, N. M.; Zhang, Y. *Proc. Natl. Acad. Sci. U.S.A.* **2012**, *109*, 8483. (n) Wang, Y.-F.; Liu, G.-Y.; Sun, L.-D.; Xiao, J.-W.; Zhou, J.-C.; Yan, C.-H. *ACS Nano* **2013**, *7*, 7200. (o) Chen, G.; Ohulchanskyy, T. Y.; Liu, S.; Law, W.-C.; Wu, F.; Swihart, M. T.; Ågren, H.; Prasad, P. N. *ACS Nano* **2012**, *6*, 2969. (p) Wang, X.; Chen, J. T.; Zhu, H.; Chen, X.; Yan, X. P. *Anal. Chem.* **2013**, *85*, 10225. (q) Wang, M.; Mi, C.-C.; Wang, W.-X.; Liu, C.-H.; Wu, Y.-F.; Xu, Z.-R.; Mao, C.-B.; Xu, S.-K. *ACS Nano* **2009**, *3*, 1580. (r) Wang, R.; Li, X.; Zhou, L.; Zhang, F. *Angew. Chem., Int. Ed.* **2014**, *53*, 12086. (s) Zhou, J.; Liu, Q.; Feng, W.; Sun, Y.; Li, F. *Chem. Rev.* **2015**, *115*, 395. (t) Chen, G.; Qiu, H.; Prasad, P.; Chen, X. *Chem. Rev.* **2014**, *114*, 5161.

(3) (a) Wang, F.; Deng, R.; Wang, J.; Wang, Q.; Han, Y.; Zhu, H.; Chen, X.; Liu, X. *Nat. Mater.* **2011**, *10*, 968. (b) Cheung, E. N. M.; Alvares, R. D. A.; Oakden, W.; Chaudhary, R.; Hill, M. L.; Pichaandi, J.; Mo, G. C. H.; Yip, C.; Macdonald, P. M.; Stanisz, G. J.; van Veggel, F. C. J. M.; Prosser, R. S. *Chem. Mater.* **2010**, *22*, 4728. (c) Su, Q.; Han, S.; Xie, X.; Zhu, H.; Chen, H.; Chen, C.-K.; Liu, R.-S.; Chen, X.; Wang, F.; Liu, X. *J. Am. Chem. Soc.* **2012**, *134*, 20849. (d) Park, Y. I.; Kim, J. H.; Lee, K. T.; Jeon, K.-S.; Na, H. B.; Yu, J. H.; Kim, H. M.; Lee, N.; Choi, S. H.; Baik, S.-I.; Kim, H.; Park, S. P.; Park, B.-J.; Kim, Y. W.; Lee, S. H.; Yoon, S.-Y.; Song, I. C.; Moon, W. K.; Suh, Y. D.; Hyeon, T. *Adv. Mater.* **2009**, *21*, 4467. (e) Xing, H.; Bu, W.; Zhang, S.; Zheng, X.; Li, M.; Chen, F.; He, Q.; Zhou, L.; Peng, W.; Hua, Y.; Shi, J. *Biomaterials* **2012**, *33*, 1079. (f) Liu, Z.; Pu, F.; Huang, S.; Yuan, Q.; Ren, J.; Qu, X. *Biomaterials* **2013**, *34*, 1712. (g) Zeng, S.; Tsang, M.-K.; Chan, C.-F.; Wong, K.-L.; Hao, J. *Biomaterials* **2012**, *33*, 9232. (h) Liu, C.; Gao, Z.; Zeng, J.; Hou, Y.; Fang, F.; Li, Y.; Qiao, R.; Shen, L.; Lei, H.; Yang, W.; Gao, M. *ACS Nano* **2013**, *7*, 7227. (i) Ju, Q.; Tu, D.; Liu, Y.; Li, R.; Zhu, H.; Chen, J.; Chen, Z.; Huang, M.; Chen, X. *J. Am. Chem. Soc.* **2012**, *134*, 1323.

(4) (a) Park, Y. I.; Kim, H. M.; Kim, J. H.; Moon, K. C.; Yoo, B.; Lee, K. T.; Lee, N.; Choi, Y.; Park, W.; Ling, D.; Na, K.; Moon, W. K.; Choi, S. H.; Park, H. S.; Yoon, S.-Y.; Suh, Y. D.; Lee, S. H.; Hyeon, T. *Adv. Mater.* **2012**, *24*, 5755. (b) Fan, W.; Shen, B.; Bu, W.; Chen, F.; Zhao, K.; Zhang, S.; Zhou, L.; Peng, W.; Xiao, Q.; Xing, H.; Liu, J.; Ni, D.; He, Q.; Shi, J. *J. Am. Chem. Soc.* **2013**, *135*, 6494. (c) Cheng, L.; Yang, K.; Li, Y.; Chen, J.; Wang, C.; Shao, M.; Lee, S.-T.; Liu, Z. *Angew. Chem., Int. Ed.* **2011**, *50*, 7385. (d) Min, Y.; Li, J.; Liu, F.; Yeow, E. K. L.; Xing, B. *Angew. Chem., Int. Ed.* **2014**, *53*, 1012. (e) Idris, N. M.; Gnanasammandhan, M. K.; Zhang, J.; Ho, P. C.; Mahendran, R.; Zhang, Y. *Nat. Med.* **2012**, *18*, 1580. (f) Lee, J.; Lee, T. S.; Ryu, J.; Hong, S.; Kang, M.; Im, K.; Kang, J. H.; Lim, S. M.; Park, S.; Song, R. *J. Nucl. Med.* **2013**, *54*, 96. (g) Li, X.; Zhou, L.; Wei, Y.; El-Toni, A. M.; Zhang, F.; Zhao, D. *J. Am. Chem. Soc.* **2014**, *136*, 15086. (h) Li, L. L.; Wu, P.; Hwang, K.; Lu, Y. *J. Am. Chem. Soc.* **2013**, *135*, 2411.

(5) (a) Hou, Y.; Qiao, R.; Fang, F.; Wang, X.; Dong, C.; Liu, K.; Liu, C.; Liu, Z.; Lei, H.; Wang, F.; Gao, M. *ACS Nano* **2012**, *7*, 330. (b) Liu, Q.; Sun, Y.; Yang, T.; Feng, W.; Li, C.; Li, F. *J. Am. Chem. Soc.* **2011**, *133*, 17122. (c) Yu, X.-F.; Sun, Z.; Li, M.; Xiang, Y.; Wang, Q.-Q.; Tang, F.; Wu, Y.; Cao, Z.; Li, W. *Biomaterials* **2010**, *31*, 8724. (d) Jin, J.; Gu, Y.-J.; Man, C. W.-Y.; Cheng, J.; Xu, Z.; Zhang, Y.; Wang, H.; Lee, V. H.-Y.; Cheng, S. H.; Wong, W.-T. *ACS Nano* **2011**, *5*, 7838. (e) Zhou, J.-C.; Yang, Z.-L.; Dong, W.; Tang, R.-J.; Sun, L.-D.; Yan, C.-H. *Biomaterials* **2011**, *32*, 9059. (f) Naczynski, D. J.; Andelman, T.; Pal, D.; Chen, S.;

DOI: 10.1021/jacs.5b00981
J. Am. Chem. Soc. XXXX, XXX, XXX−XXX

Riman, R. E.; Roth, C. M.; Moghe, P. V. *Small* **2010**, *6*, 1631. (g) Yang, Y.; Sun, Y.; Cao, T.; Peng, J.; Liu, Y.; Wu, Y.; Feng, W.; Zhang, Y.; Li, F. *Biomaterials* **2013**, *34*, 774. (h) Xing, H.; Bu, W.; Ren, Q.; Zheng, X.; Li, M.; Zhang, S.; Qu, H.; Wang, Z.; Hua, Y.; Zhao, K.; Zhou, L.; Peng, W.; Shi, J. *Biomaterials* **2012**, *33*, 5384. (i) Jang, G. H.; Hwang, M. P.; Kim, S. Y.; Jang, H. S.; Lee, K. H. *Biomaterials* **2014**, *35*, 440. (j) Chen, G.; Shen, J.; Ohulchanskyy, T. Y.; Patel, N. J.; Kutikov, A.; Li, Z.; Song, J.; Pandey, R. K.; Ågren, H.; Prasad, P. N.; Han, G. *ACS Nano* **2012**, *6*, 8280. (k) Sun, Y.; Feng, W.; Yang, P.; Huang, C.; Li, F. *Chem. Soc. Rev.* **2015**, *44*, 1509.

(6) (a) Li, R.; Ji, Z.; Dong, J.; Chang, C. H.; Wang, X.; Sun, B.; Wang, M.; Liao, Y.-P.; Zink, J.; Nel, A.; Xia, T. *ACS Nano* **2015**, *9*, 3293. (b) Bergman, L.; Kankaanpää, P.; Tiitta, S.; Duchanoy, A.; Li, L.; Heino, J.; Lindén, M. *Mol. Pharmaceutics* **2013**, *10*, 1795.

(7) (a) Lewinski, N.; Colvin, V.; Drezek, R. *Small* **2008**, *4*, 26. (b) Belyanskaya, L.; Manser, P.; Spohn, P.; Bruinink, A.; Wick, P. *Carbon* **2007**, *45*, 2643. (c) Sims, J. T.; Plattner, R. *Cancer Chemother. Pharmacol.* **2009**, *64*, 629. (d) Wang, P.; Henning, S. M.; Heber, D. *PLoS One* **2010**, *5*, e10202. (e) Monteiro-Riviere, N. A.; Inman, A. O.; Zhang, L. W. *Toxicol. Appl. Pharmacol.* **2009**, *234*, 222.

(8) (a) Soenen, S. J.; Demeester, J.; De Smedt, S. C.; Braeckmans, K. *Nano Today* **2013**, *8*, 121. (b) Zhang, Y.; Zheng, F.; Yang, T.; Zhou, W.; Liu, Y.; Man, N.; Zhang, L.; Jin, N.; Dou, Q.; Zhang, Y.; Li, Z.; Wen, L.-P. *Nat. Mater.* **2012**, *11*, 817. (c) Wu, Y. N.; Yang, L. X.; Shi, X. Y.; Li, I. C.; Biazik, J. M.; Ratinac, K. R.; Chen, D. H.; Thordarson, P.; Shieh, D. B.; Braet, F. *Biomaterials* **2011**, *32*, 4565. (d) Peynshaert, K.; Manshian, B. B.; Joris, F.; Braeckmans, K.; De Smedt, S. C.; Demeester, J.; Soenen, S. J. *Chem. Rev.* **2014**, *114*, 7581.

(9) Bogdan, N.; Vetrone, F.; Ozin, G. A.; Capobianco, J. A. *Nano Lett.* **2011**, *11*, 835.

(10) (a) Kroemer, G.; Galluzzi, L.; Vandenabeele, P.; Abrams, J.; Alnemri, E. S.; Baehrecke, E. H.; Blagosklonny, M. V.; El-Deiry, W. S.; Golstein, P.; Green, D. R.; Hengartner, M.; Knight, R. A.; Kumar, S.; Lipton, S. A.; Malorni, W.; Nunez, G.; Peter, M. E.; Tschopp, J.; Yuan, J.; Piacentini, M.; Zhivotovsky, B.; Melino, G. *Cell Death Differ.* **2009**, *16*, 3. (b) Fink, S. L.; Cookson, B. T. *Infect. Immun.* **2005**, *73*, 1907.

(11) Levine, B.; Yuan, J. *J. Clin. Invest.* **2005**, *115*, 2679.

(12) (a) Klionsky, D. J.; Abdalla, F. C.; Abeliovich, H.; Abraham, R. T.; Acevedo-Arozena, A.; Adeli, K.; Agholme, L.; Agnello, M.; Agostinis, P.; Aguirre-Ghiso, J. A. *Autophagy* **2012**, *8*, 445. (b) Klionsky, D. J.; Cuervo, A. M.; Seglen, P. O. *Autophagy* **2007**, *3*, 181.

(13) (a) Eskelinen, E.-L. *Autophagy* **2005**, *1*, 1. (b) Tasdemir, E.; Galluzzi, L.; Maiuri, M. C.; Criollo, A.; Vitale, I.; Hangen, E.; Modjtahedi, N.; Kroemer, G. *Methods Mol. Biol.* **2008**, *445*, 29.

(14) (a) Hussain, S.; Al-Nsour, F.; Rice, A. B.; Marshburn, J.; Yingling, B.; Ji, Z.; Zink, J. I.; Walker, N. J.; Garantziotis, S. *ACS Nano* **2012**, *6*, 5820. (b) Cui, Q.; Tashiro, S.; Onodera, S.; Minami, M.; Ikejima, T. *Biol. Pharm. Bull.* **2007**, *30*, 859. (c) Amaral, C.; Borges, M.; Melo, S.; Silva, E. T. d.; Correia-da-Silva, G.; Teixeira, N. *PLoS One* **2012**, *7*, e42398. (d) Abedin, M. J.; Wang, D.; McDonnell, M. A.; Lehmann, U.; Kelekar, A. *Cell Death Differ.* **2007**, *14*, 500.

(15) (a) Bratton, D. L.; Fadok, V. A.; Richter, D. A.; Kailey, J. M.; Guthrie, L. A.; Henson, P. M. *J. Biol. Chem.* **1997**, *272*, 26159. (b) Martin, S. J.; Reutelingsperger, C. P.; McGahon, A. J.; Rader, J. A.; van Schie, R. C.; LaFace, D. M.; Green, D. R. *J. Exp. Med.* **1995**, *182*, 1545. (c) Logue, S. E.; Elgendy, M.; Martin, S. J. *Nat. Protoc.* **2009**, *4*, 1383. (d) Zwaal, R. F.; Comfurius, P.; Bevers, E. M. *Cell. Mol. Life Sci.* **2005**, *62*, 971.

(16) Elmore, S. *Toxicol. Pathol.* **2007**, *35*, 495.

(17) Kajstura, M.; Halicka, H. D.; Pryjma, J.; Darzynkiewicz, Z. *Cytometry, Part A* **2007**, *71A*, 125.

(18) (a) Zhang, P.; Ma, Y.; Zhang, Z.; He, X.; Guo, Z.; Tai, R.; Ding, Y.; Zhao, Y.; Chai, Z. *Environ. Sci. Technol.* **2011**, *46*, 1834. (b) Ma, Y.; He, X.; Zhang, P.; Zhang, Z.; Guo, Z.; Tai, R.; Xu, Z.; Zhang, L.; Ding, Y.; Zhao, Y.; Chai, Z. *Nanotoxicology* **2011**, *5*, 743. (c) Li, R.; Ji, Z.; Chang, C. H.; Dunphy, D. R.; Cai, X.; Meng, H.; Zhang, H.; Sun, B.; Wang, X.; Dong, J.; Lin, S.; Wang, M.; Liao, Y.-P.; Brinker, C. J.; Nel, A.; Xia, T. *ACS Nano* **2014**, *8*, 1771.

DOI: 10.1021/jacs.5b00981
J. Am. Chem. Soc. XXXX, XXX, XXX−XXX